Electronic Supplementary Information

NO release regulated by doxorubicin as green light-harvesting antenna

Aurore Fraix, ‡[a] Cristina Parisi,‡[a] Mariacristina Failla,‡[a,b] Konstantin Chegaev,[b] Francesca Spyrakis,[b] Loretta Lazzarato,*[b] Roberta Fruttero,[b] Alberto Gasco[b] and Salvatore Sortino*[a]

[a]*Laboratory of Photochemistry, Department of Drug Sciences, University of Catania, I-95125 Catania, Italy.*
E-mail: ssortino@unict.it
[b]*Department of Drug Science and Technology, University of Torino, 10125 Torino, Italy.*
E-mail: loretta.lazzarato@unito.it

Chemicals

All chemicals were purchased by Sigma-Aldrich and used as received. The concentrations of ct-DNA, in base pair (bp), was determined by absorption spectroscopy, using a molar extinction coefficient of 13,200 M^{-1} cm^{-1} at 260 nm.[1S] Organic solvents were removed under reduced pressure at 30 °C. Synthetic-purity solvents were used. All solvents used for the spectrophotometric studies were spectrophotometric grade.

Instrumentation

^{1}H and ^{13}C NMR spectra were recorded on a Varian UNITY Inova at 500 MHz. Chemical shifts (δ) are given in parts per million (ppm) and the coupling constants (*J*) are given in Hz. The following abbreviations are used to designate peak multiplicity: s = singlet, d = doublet, dd = doublet of doublets, t = triplet, td = triplet of doublets, m = multiplet. Low resolution mass spectra were recorded on a Micromass Quattro micro™ API (Waters Corporation, Milford, MA, USA) with electrospray ionization. Flash column chromatography was performed on silica gel (Merck Kieselgel 60, 230-400 mesh ASTM). The progress of the reactions was followed by thin layer chromatography (TLC) on 5×20 cm plates with a layer thickness of 0.2 mm. The purity of target compound was assessed by RP-HPLC. Analyses were performed on a HP1100 chromatograph system (Agilent Technologies, Palo Alto, CA, USA) equipped with a quaternary pump (G1311A), a membrane degasser (G1379A), a diode-array detector (DAD) (G1315B) integrated in the HP1100 system. Data analysis were processed by HP ChemStation system (Agilent Technologies). The analytical column was a LiChrospher RP-18e 100 A (250 × 4.6 mm, 5 μm particle size) (Merck, Darmstadt, Germany). The mobile phase consisting of acetonitrile (A)/0.1% trifluoroacetic acid (B), in gradient mode (35% A until 5 min, from 35 to 80% A between 5 and 8 min, 80% A between 8 and 15 min, and from 80 to 35% A between 15 and 18 min) at the flow-rate of 1 mL/min. The injection volume was 20 μL (Rheodyne, Cotati, CA). The column effluent was monitored at 234, 254, and 480 mn referenced against at 800 nm wavelength. Data analysis was performed with Agilent ChemStation.

UV-Vis spectra absorption and fluorescence emission spectra were recorded with a Perkin Elmer spectrophotometer (mod. Lambda 365) and a Spex Fluorolog-2 (mod. F-111) spectrofluorimeter, respectively, using either quartz cells with a path length of 1 cm. Fluorescence lifetimes were recorded with the same fluorimeter equipped with a TCSPC Triple Illuminator. The samples were irradiated by a pulsed diode excitation source Nanoled at 455 nm. The kinetics were monitored at 525 and 530 nm and ethanol solution itself was used to register the prompt at 455 nm. The system allowed measurement of fluorescence lifetimes from 200 ps. The multi-exponential fit of the fluorescence decay was obtained using equation (1):

$$I(t) = \Sigma\alpha_i \exp(^{-t/\tau i}) \quad (1)$$

Photolysis experiments were performed by irradiating the samples in solution in a thermostated quartz cell (1 cm pathlength, 3 mL capacity) under gentle stirring, by using a 200 mW continuum laser (λ_{exc} = 532 nm) having a beam diameter of ca. 1.5 mm. The photolysis experiments under anaerobic conditions were performed

deoxygenating the solution by bubbling with a vigorous and constant flux of pure nitrogen (previously saturated with solvent).

Direct monitoring of NO release for samples in solution was performed by amperometric detection with a World Precision Instrument, ISO-NO meter, equipped with a data acquisition system, and based on direct amperometric detection of NO with short response time (< 5 s) and sensitivity range 1 nM – 20 μM. The analog signal was digitalized with a four-channel recording system and transferred to a PC. The sensor was accurately calibrated by mixing standard solutions of $NaNO_2$ with 0.1 M H_2SO_4 and 0.1 M KI according to the reaction:

$$4H^+ + 2I^- + 2NO_2^- \rightarrow 2H_2O + 2NO + I_2$$

Irradiation was performed in a thermostated quartz cell (1 cm pathlength, 3 mL capacity) using the above continuum laser with λ_{exc} = 532 nm. NO measurements were carried out under stirring with the electrode positioned outside the light path in order to avoid NO signal artefacts due to photoelectric interference on the ISO-NO electrode.

Laser flash photolysis. All solutions were excited with the second harmonic of Nd–YAG Continuum Surelite II–10 laser (532 nm, 6 ns FWHM), using quartz cells with path length 1.0 cm. The excited solutions were analyzed with a Luzchem Research mLFP–111 apparatus with an orthogonal pump/probe configuration. The probe source was a ceramic xenon lamp coupled to quartz fibre-optic cables. The laser pulse and the mLFP–111 system were synchronized by a Tektronix TDS 3032 digitizer, operating in pre-trigger mode. The signals from a compact Hamamatsu photomultiplier were initially captured by the digitizer and then transferred to a personal computer, controlled by Luzchem Research software operating in the National Instruments LabView 5.1 environment. The solutions were deoxygenated by bubbling with a vigorous and constant flux of pure nitrogen (previously saturated with solvent). The solution temperature was 295 ± 2 K. The energy of the laser pulse was measured at each shot with a SPHD25 Scientech pyroelectric meter.

Synthesis and characterization

DXNO-BL was synthesized according to our already reported procedure.[2S] **DXNO-GR** was synthesized according to the procedure reported in Scheme S1. Briefly compound **a2** was obtained through nitrosation of **a1** with $NaNO_2$ and CH_3COOH. All syntheses were carried out under a low intensity level of visible light. Compound **1** was prepared from a mixture of 14-bromo and 14-chlorodaunorubicine hydrobromide **a3** and compound **a2**; the reaction was performed in dry DMF in presence of KF at room temperature. After purification by flash chromatography, the product was isolated as hydrochloride. Compound **a1** and compound **a3** were synthetized according to literature.[2S,3S]

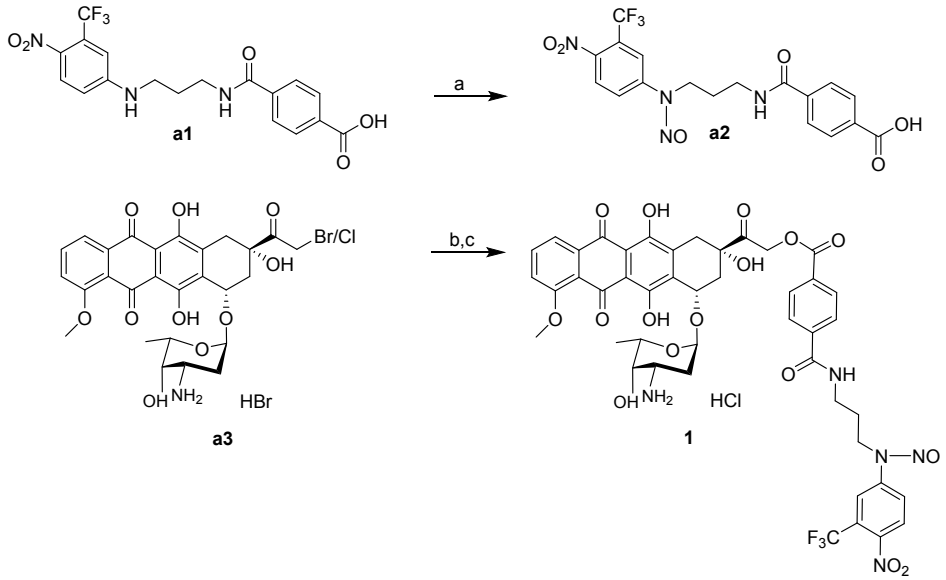

Scheme S1 a) $NaNO_2$, CH_3COOH/THF 1/1, r.t.; b) **a2**, KF, DMF, rt; c) THF, HCl in dry dioxane.

4-((3-((4-Nitro-3-(trifluoromethyl)phenyl)(nitroso)amino)propyl)carbamoyl)benzoic acid (a2).

To a solution of **a1** (760 mg, 1.85 mmol) in a mixture THF/CH_3COOH (1/1 v/v; 150 mL) cooled at 0 °C with an ice bath, sodium nitrite (1 g, 14.78 mmol) was added; the reaction mixture was stirred at 0 °C for 2 h. Then, the mixture was stirred for another 12 h at room temperature. When the reaction was completed (TLC), the obtained mixture was diluted with DCM and washed with water (3 × 20 mL), dried over Na_2SO_4 and concentrated to dryness. Purification of the residue by flash chromatography, using CH_2Cl_2/MeOH (95/5 v/v) as the eluent, gave the target compound as a yellow solid (474 mg, 58%). ESI MS $[M-H]^-$: 439.

Doxorubicin 4-((3-((4-nitro-3 (trifluoromethyl)phenyl)(nitroso)amino)propyl)carbamoyl)benzoate (DXNO-GR).

To a stirred solution of **a2** (366 mg, 0.83 mmol) in dry DMF, KF (96 mg, 1.66 mmol) was added in one portion, and the reaction was vigorously stirred for 15 min. 14-Bromo/chloro daunorubicin hydrobromide **a3** (184 mg, 0.28 mmol) was added and the reaction was stirred at rt for 4 h. Solvent was removed under reduced pressure at 30°C and the resulting mixture was purified by flash chromatography CH_2Cl_2/MeOH (95/5 to 80/20 v/v) as the eluent to give a dark-red solid. The resulting compound was suspended in dry THF (10 mL), and 2 equivalents of HCl solution in dry dioxane were added. The resulting mixture was stirred for 1 h at rt and then diluted with Et_2O.

The resulting precipitate was filtered, washed with Et_2O and dried under vacuum to give the title compound as a red powder (123 mg, 44%). Purity: 96%. ESI MS $[M+H]^+$: 966.

^{1}H NMR (500 MHz, DMSO-d_6) δ 8.68 (t, J = 5.6 Hz, 1H, CONH), 8.33 (d, J = 8.8 Hz, 1H, CHAr), 8.23 (d, J = 2.4 Hz, 1H, CHAr), 8.20 (dd, J = 8.8, 2.4 Hz, 1H, CHAr), 8.07 (d, J = 8.2 Hz, 2H, CHAr), 7.94 (d, J = 8.2 Hz, 2H, CHAr), 7.92 (d, J = 4.6 Hz, 2H, ^{1}CHAr , ^{3}CHAr), 7.66 (t, J = 5.2, 4.6 Hz, 1H, ^{2}CHAr), 5.76 (s, 1H, ^{9}COH), 5.57 – 5.44 (m, 2H, $^{14}CH_2$), 5.30 (d, J = 3.5 Hz, 1H, $^{1'}$CH), 4.99 (dd, J = 5.5, 2.9 Hz, 1H, ^{7}CH), 4.23 (m, 3H, $^{5'}$CH, -CH_2CH_2**CH_2**-N(NO)), 3.98 (s, 3H, -OCH_3), 3.57 (s, 1H, $^{4'}$CH**OH**), 3.25 (m, 2H, -**CH_2**CH_2CH_2-

), 3.12 (d, J = 18.1 Hz, 1H, $^{10}CH_2$), 2.95 (d, J = 18.1 Hz, 1H, $^{10}CH_2$), 2.38 – 2.32 (m, 1H, $^{8}CH_2$), 2.13 (m, 1H, $^{8}CH_2$), 1.88 (td, J = 12.7, 3.8 Hz, 1H, $^{2'}CH$), 1.78 – 1.64 (m, 3H, -CH_2**C**$\mathbf{H_2}$$CH_2$-, $^{3'}CH$), 1.19 (d, J = 6.5 Hz, 3H, $^{6'}CH_3$).

^{13}C NMR (125 MHz, DMSO-d_6) δ 207.70, 206.18, 188.63, 186.51, 165.34, 164.69, 160.83, 155.94, 150.25, 144.44, 138.72, 136.30, 135.15, 134.76, 133.85, 131.15, 129.26, 127.58, 127.55, 123.42, 123.41, 120.02, 117.85, 117.80, 110.82, 110.73, 99.33, 75.21, 69.64, 66.61, 66.22, 56.62, 46.60, 40.49, 40.02, 36.89, 36.16, 31.93, 28.51, 28.47, 25.77, 16.68.

^{1}H

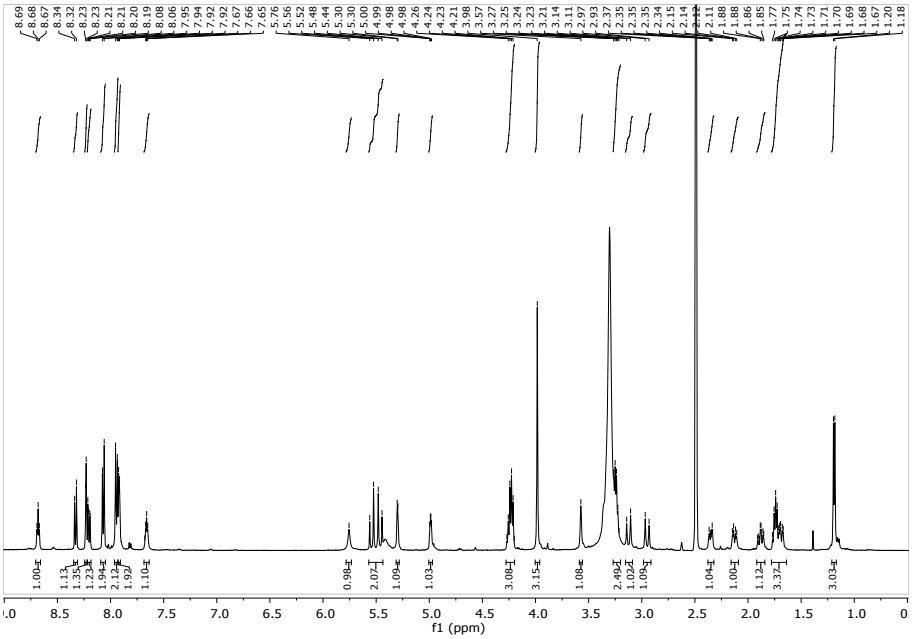

^{13}C

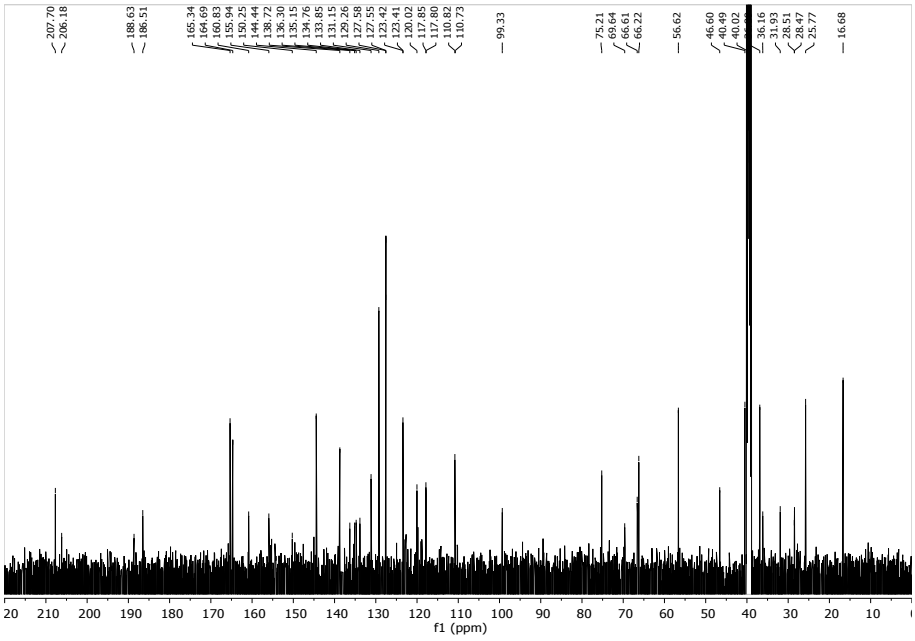

COSY

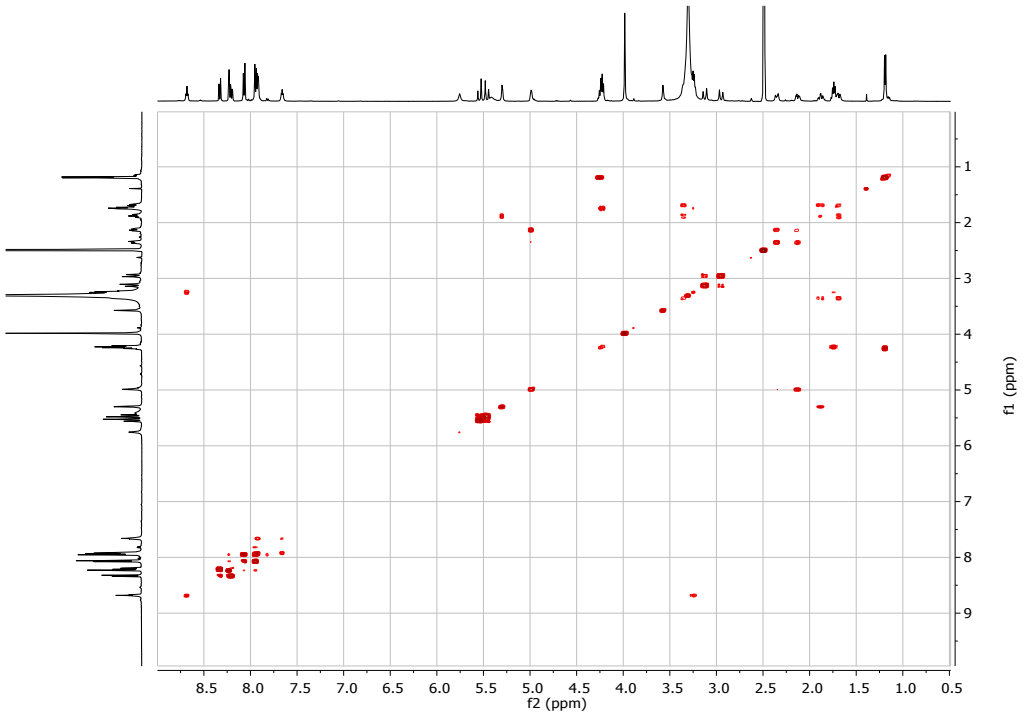

HSCQ

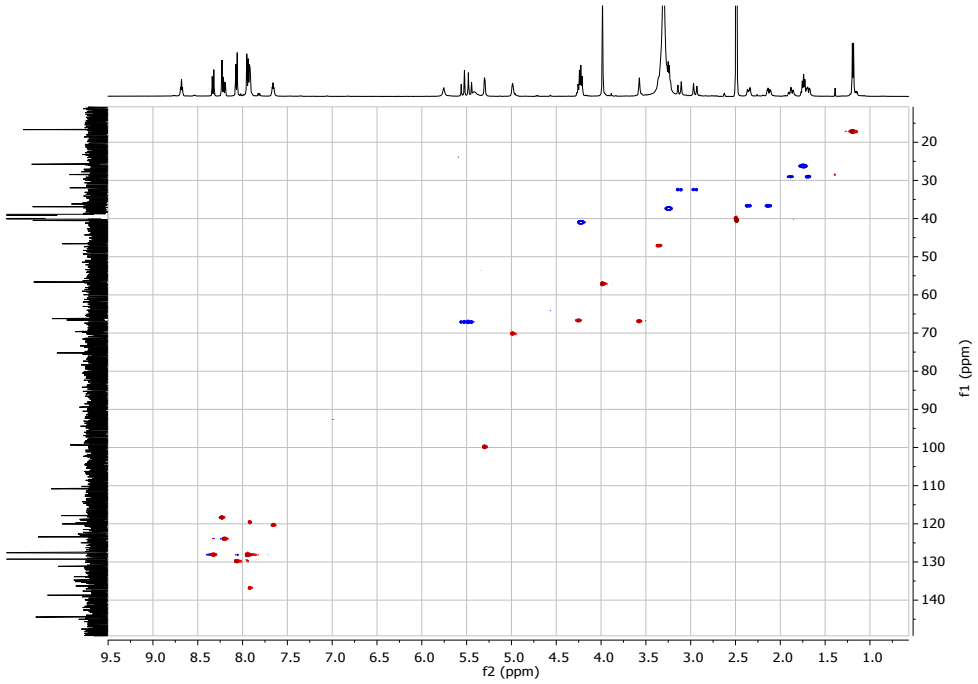

Fluorescence quantum yields

Fluorescence quantum yields were determined using optically-matched solutions at the excitation wavelength of **DXNO-GR**, and a solution of Rhodamine 6G in EtOH as standard ($\Phi_f = 0.94$)[4S] through equation (2):

$$\Phi_f = \Phi_{f(s)} (In^2/I_{(s)}n^2_{(s)}) \qquad (2)$$

where $\Phi_{f(s)}$ is the fluorescence quantum yield of the standard; I and $I_{(s)}$ are the areas of the fluorescence spectra of compounds and standard, respectively; n and $n_{(s)}$ are the refraction index of the solvents used for compounds and standard. Absorbance at the excitation wavelength was less than 0.1 in all cases.

Determination of the DNA binding parameters

The half-reciprocal plot fitted fairly well the data of Figure 3A according to equation (3):[5S]

$$[\text{ct-DNA}]_{bp}/(\varepsilon_A-\varepsilon_F) = [\text{ct-DNA}]_{bp}/(\varepsilon_B-\varepsilon_F) + 1/K_b(\varepsilon_B-\varepsilon_F) \quad (3)$$

where $[\text{ct-DNA}]_{bp}$ is the concentration of the polynucleotide in base pairs, ε_A, ε_F, ε_B correspond to $A_{obs}/[$ **DXNO-GR**], the extinction coefficient for the free **1** and the extinction coefficient for the totally bound form of **DXNO-GR**, respectively.[5S] By the ratio of the slope to intercept of the linear plot reported in Fig. S7 a K_b value of $\approx 3x10^5$ $M^{-1}s^{-1}$ was obtained. This value is good agreement with the value obtained by the Stern-Volmer plot of the fluorescence data, according to equation (4):[6S]

$$I_0/I = 1 + K_{SV}[\text{ct-DNA}]_{bp} \qquad (4)$$

where I_0 and I are the fluorescence intensities in the absence and in the presence of ct-DNA, respectively, and K_{SV} is the Stern-Volmer equation. As reported in the text, the emission features observed in the presence of ct-DNA accords well with a static quenching mechanism. Under these conditions, the K_{SV} value obtained from the linear part of the plot (Fig. S8), identifies with the K_b, providing a value of $K_b \approx 3x10^5$ $M^{-1}s^{-1}$. The positive deviation from the Stern-Volmer equation observed in Fig. S8 is not surprising since it is very common whenever the extent of quenching is large,[6S] as in our case.

The fluorescence data were also useful to calculate the value of *n* which represent the number of binding sites for each molecule of **DXNO-GR**, by applying equation (5): [7S]

$$\log [(I_0 - I)/I] = \log K_b + n\log[\text{ct-DNA}]_{bp} \qquad (5)$$

From the linear part of the plot (Fig. S9) a value of $n \approx 1.5$ was obtained.

Computational details

Plain Molecular Dynamics. The most probable proromeric state of the nitrosated DOX derivative was check and assigned using Moka.[8S] The ligand was parametrized with the ab initio RESP charges fitting methodology, as implemented in the BiKi Life Science software suite.[9S,10S] The MD simulation setup was performed with BiKi. Gromacs 4.6.1 was used to run MD simulations.[11S]. The water model employed was TIP3P. The solvated system was preliminary minimized by 5000 steps of steepest descent. The integration step was equal to 1 fs. The Verlet cutoff scheme, the Bussi−Parrinello thermostat, LINCS for the constraints (all bonds), and the particle mesh Ewald for electrostatics, with a short-range cutoff of 11 Å, were applied. The system was equilibrated in four subsequent steps: 100 ps in NVT ensemble at 100 K, 100 ps in NVT ensemble at 200 K, 100 ps in NVT ensemble at 300 K, and a 1 ns long NPT simulation to reach the pressure equilibrium condition. No restraint was applied. The production run was carried out in the NVT ensemble at 300 K without any restraint for 50 ns. Two replicas were simulated upon velocity reassignment.
Upon completion of the simulation we employed the algorithm proposed in Decherchi et al.[12S] and used the backbone RMSD with optimal alignment (Kabsch algorithm) between frames as metric for distance computation, to cluster the trajectories. We obtained ten clusters for each replica and inspected the corresponding representative medoid.

Molecular Docking. The reference crystallographic structure used for static and dynamic docking simulations was retrieved from the Protein Data Bank (PDB code 1xrw). The structure originally contained a platinum acridine derivative, intercalating a DNA octamer in between G-C and C-G base pairs. The cognate ligand was removed and the binding site, thus defined, used for the following simulations.
Targeted dynamic docking was performed using the original protocol developed by BiKi Technologies[13S]: two subsets (A and B) were defined, with A being the ligand and B the G-C and C-G base pairs. 10 replicas of 20 ns each were set up, and for each run velocities were reassigned according to a Maxwell-Boltzmann distribution at 300 K. An electrostatic bias was applied until subset A reached a distance of 4 Å from subset B, then the bias was switched-off and the production was carried out as a plain MD until the end of the simulation time.

References

1S. J. K. Barton, J. M. Goldberg, C. V. Kumar and N. J. Turro, *J. Am. Chem. Soc.*, 1986, **108**, 2081.

2S. K. Chegaev, A. Fraix, E. Gazzano, G.E.F. Abd-Ellatef, M. Blangetti, Rolando, B.; S. Conoci, C. Riganti, R. Fruttero, A. Gasco, and S. Sortino, *ACS Med Chem Lett*., 2017, **8**, 361.

3S WO2004/011033, 2004.

4S M. Montalti, A. Credi, L. Prodi and M. T. Gandolfi, Handbook of Photochemistry, 3rd ed., CRC, Boca Raton, 2006.

5S A. M. Pyle, J. P. Rehmann, R. Meshoyer, C. V. Kumar, N. J. Turro and J. K. Barton, *J. Am. Chem. Soc*., 1989, **111**, 3051.

6S. J. R. Lakowicz, Principles of fluorescence spectroscopy, 2006, 3rd ed., Chapter 8, pp 282−284, Springer Science, Business Media, New York.

7S. A. Agudelo, P. Bourassa, G. Bérubé, and H.-A. Tajmir-Riahi, *Int. J. Biol. Macromol.*, 2014, **66**, 144.

8S. F. Milletti, L. Storchi, G. Sforna and G. Cruciani, *J. Chem. Inf. Model.* 2007, **47**, 2172.

9S. http://www.bikitech.com.

10S. S. Sciabola, P. Benedetti, G. D'Arrigo, R. Torella, M. Baroni, G. Cruciani and F. Spyrakis, *ACS Med. Chem. Lett.*, 2019, **10**, 487.

11S. B. Hess, C. Kutzner, D. van der Spoel and E. Lindahl, *J. Chem. Theory Comput.*, 2008, **4**, 435.

12S. S. Decherchi, A. Nerteotti, G. Bottegoni, W. Rocchia and A. Cavalli*, Nat. Commun*., 2015, **6**, 6155.

13S. S. Decherchi, G. Bottegoni, A. Spitaleri, W. Rocchia and A. Cavalli, *J Chem. Inf. Model.,* 2018, **58**, 219.

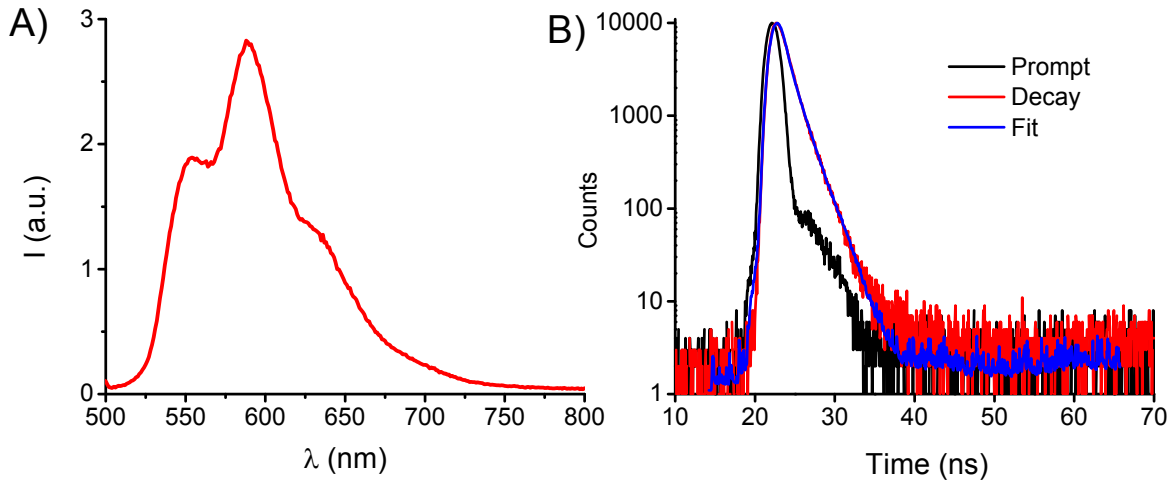

Fig. S1 Fluorescence emission spectrum, λ_{exc} = 480 nm (A) and fluorescence emission decay, λ_{exc} = 455 nm, λ_{em} = 600 nm (B) of a solution of DOX in H_2O:MeOH (20:80 v/v), T = 25 °C.

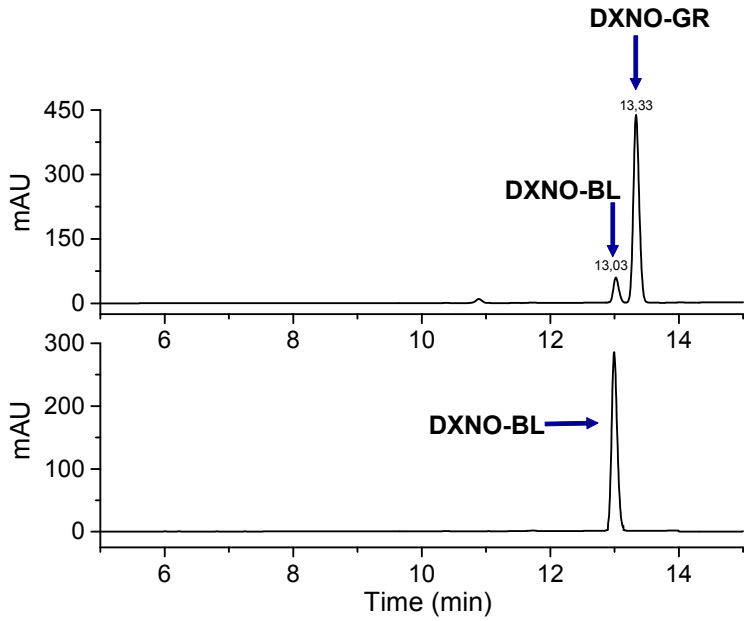

Fig. S2 HPLC traces related to solutions of **DXNO-GR** (100 µM in MeOH) after 60 min irradiation times with green light (top) and, for comparison, the authentical non nitrosate derivative **DXNO-BL** (bottom).

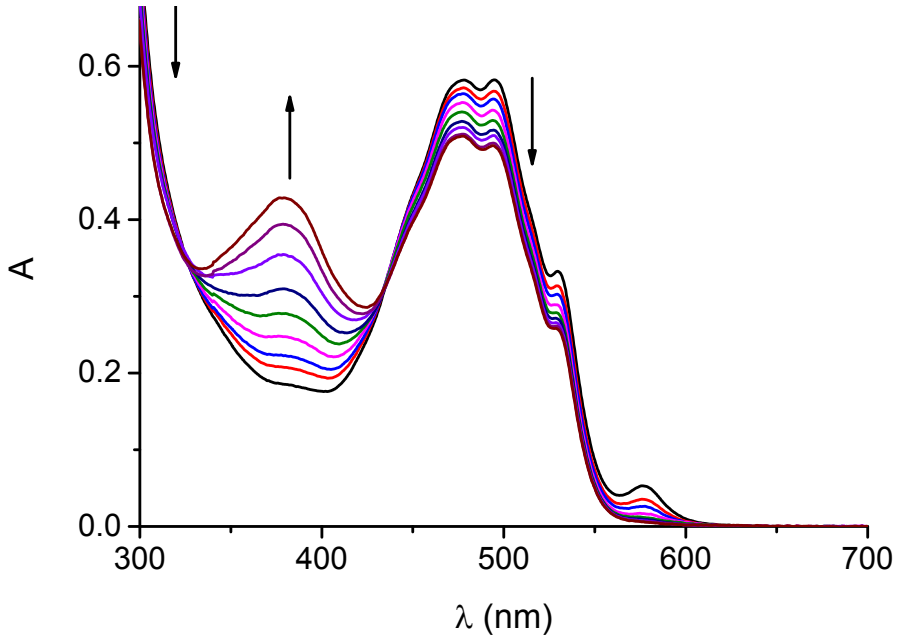

Fig. S3 Absorption spectral changes observed upon exposure of a N_2-saturated solution of **DXNO-GR** (48 μM) at λ_{exc} = 532 nm from 0 to 330 min. The arrows indicate the course of the spectral profile with the illumination time. H_2O: MeOH (20:80 v/v). T = 25 °C.

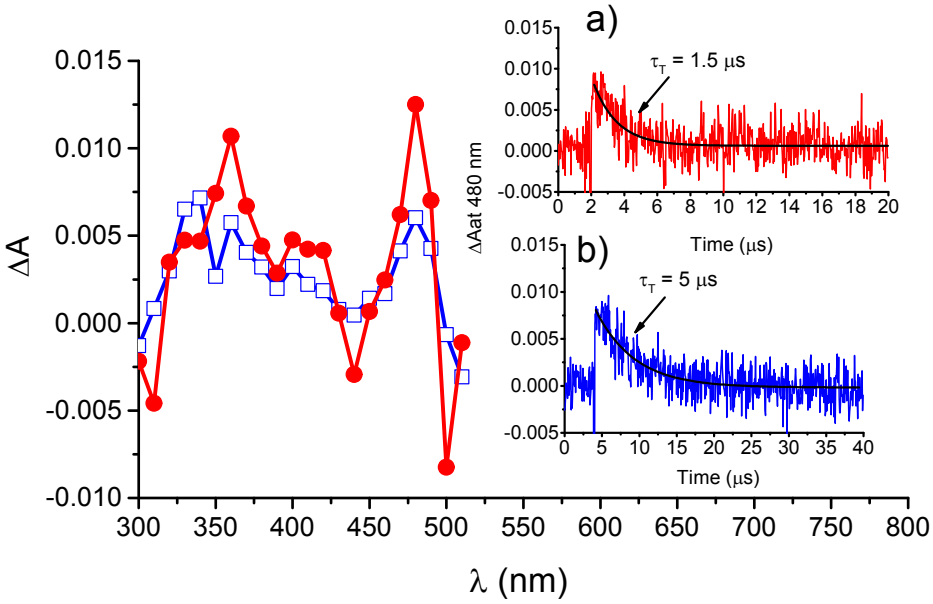

Fig. S4 Transient absorption spectra observed 0.1 μs after 532 nm laser excitation (pulse with ≈ 6 ns, E_{532} ≈ 10 mJ pulse^{-1}) of N_2-saturated solutions of **DXNO-GR** (●) and DOX (□) (48 μM) The insets show the decay traces monitored at 480 nm and the related first-order fitting for **DXNO-GR** (a) and DOX (b). H_2O: MeOH (20:80 v/v). T = 25 °C.

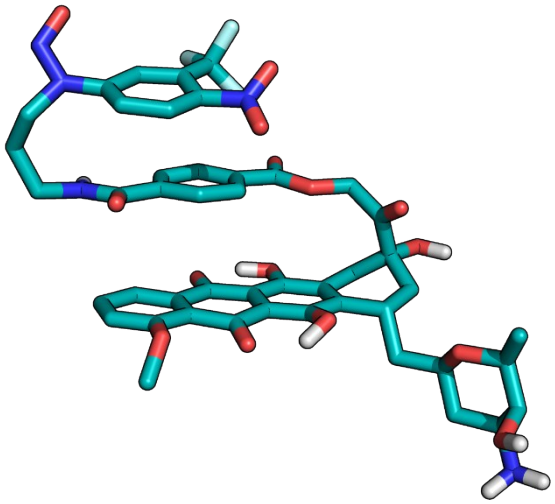

Fig. S5 Sandwich conformation assumed by the molecular hybrid **DXNO-GR** during MD simulations.

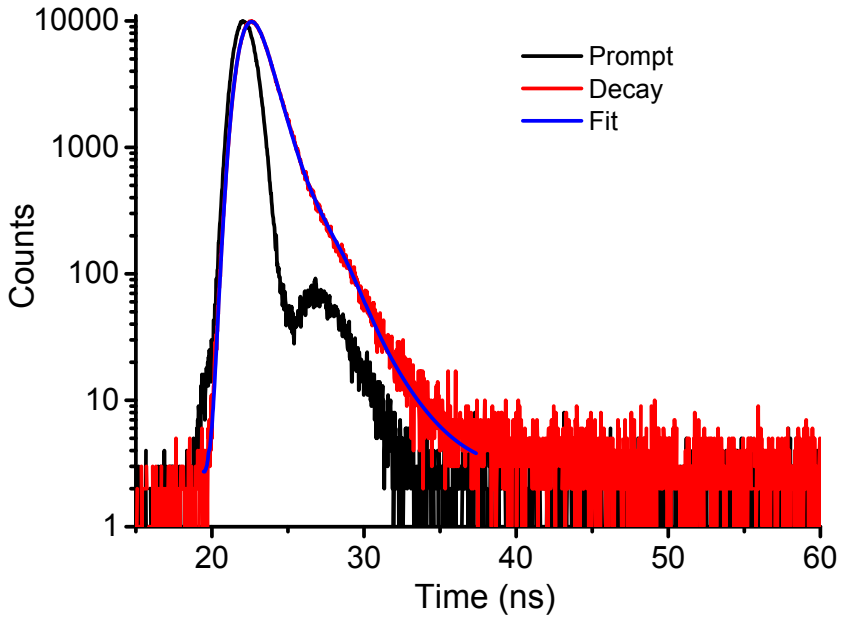

Fig. S6 Fluorescence emission (λ_{exc} = 455 nm, λ_{em} = 600 nm) of a solution of **DXNO-GR** in H_2O:DMSO (95:5 v/v),T = 25 °C.

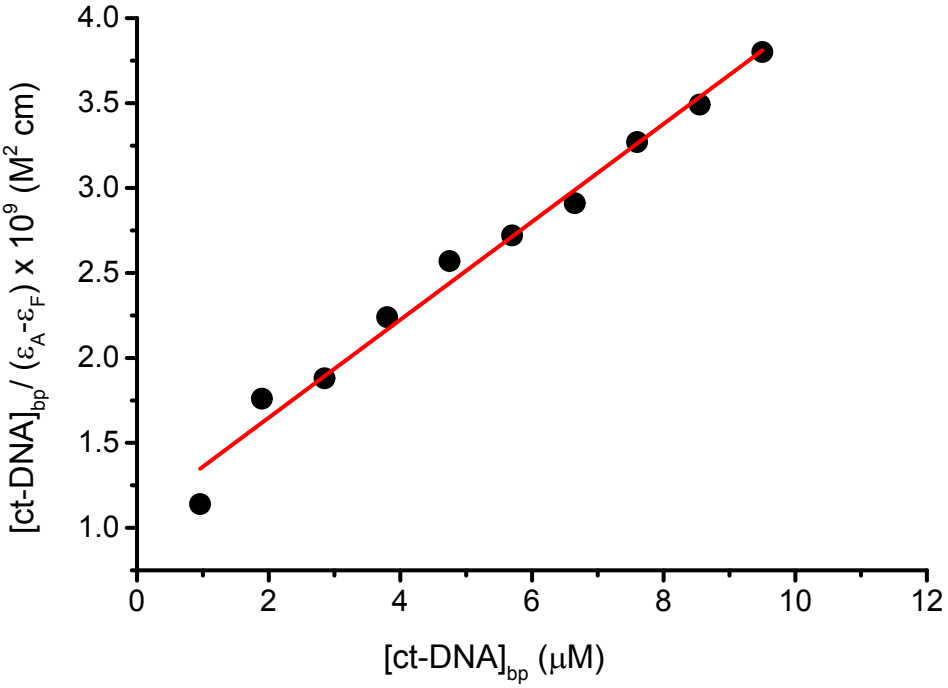

Fig. S7 Half-reciprocal plot of binding of **DXNO-GR** with ct-DNA determined using the absorbance changes reported in Fig. 3A at λ = 490 nm.

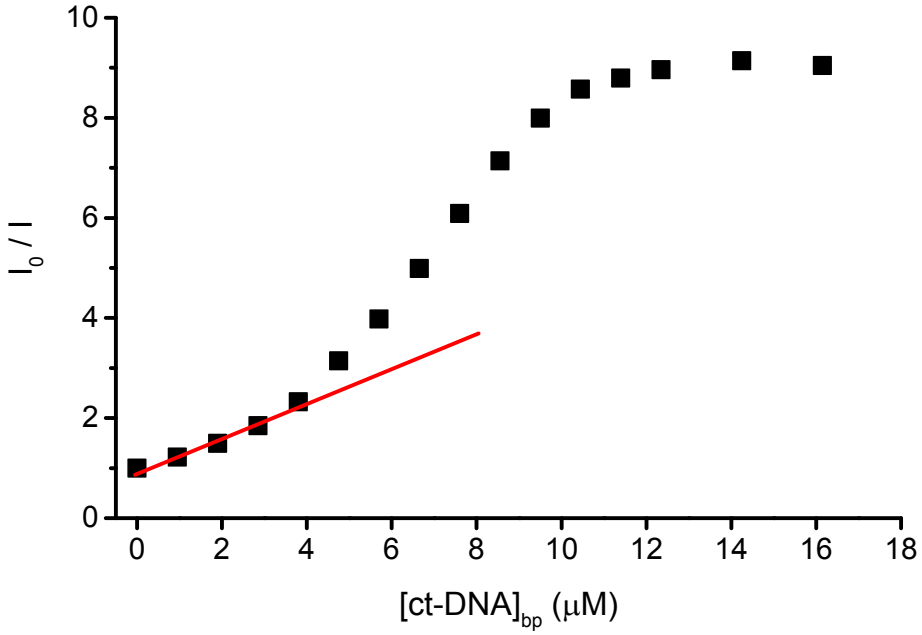

Fig. S8 Stern-Volmer plot related to the fluorescence data ct-DNA determined using the fluorescence changes reported in Fig. 3B at λ_{em} = 600 nm. The red line is the best fit according to the Stern−Volmer equation.

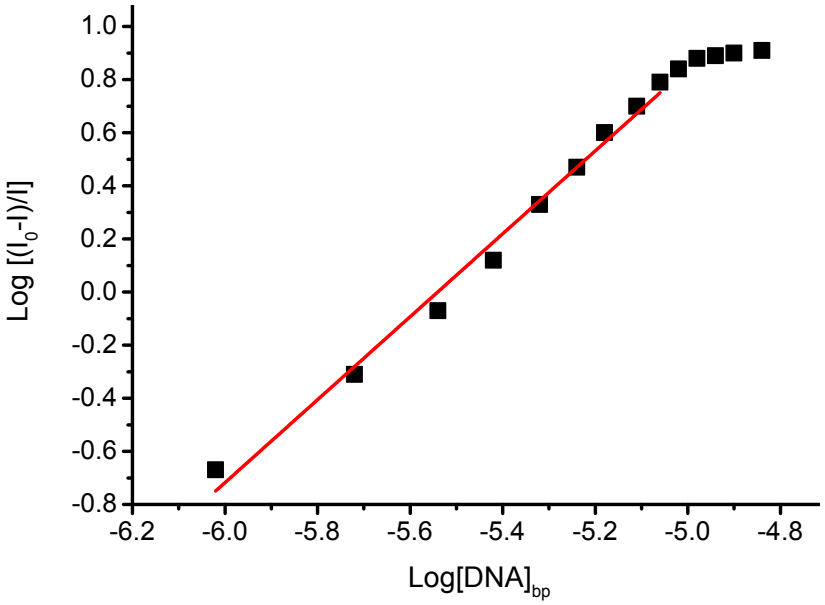

Fig. S9 Plot of $\log(I_0 - I)/I$ as a function of $\log[DNA]_{bp}$ obtained by using the fluorescence changes reported in Fig. 3B at λ_{em} = 600 nm.

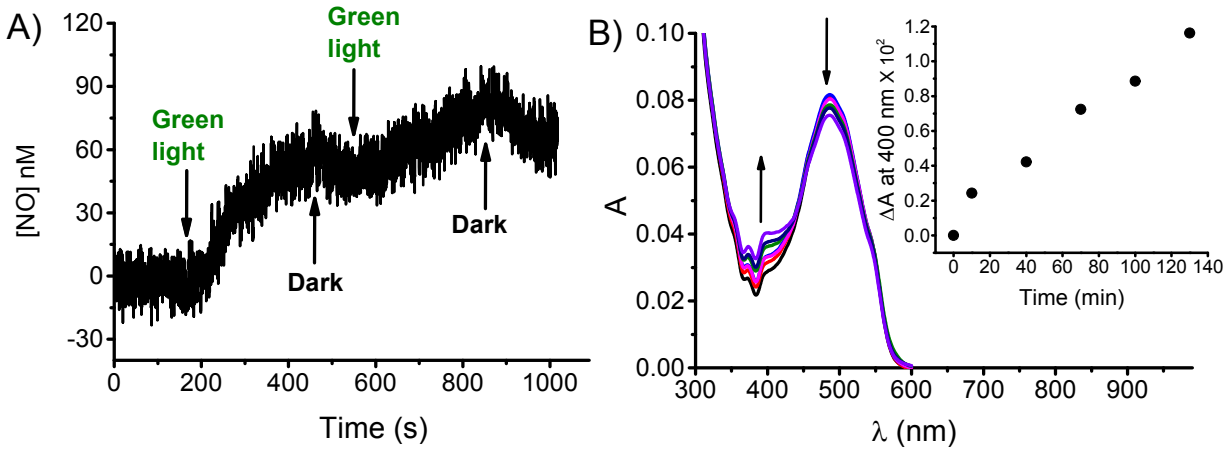

Fig. S10 (A) NO release profile observed for a solution of **DXNO-GR** (9.5 μM) in the presence of ct-DNA (20 μM) upon alternate cycles of green light (λ_{exc} = 532 nm) and dark. (B) Absorption spectral changes observed upon exposure of an air-equilibrated solution of **DXNO-GR** (9.5 μM) in the presence of ct-DNA (20 μM) at λ_{exc} = 532 nm for different time intervals. The arrows indicate the course of the spectral profile with the illumination time. The insets show the difference absorbance changes at λ = 400 nm. H_2O:DMSO (95:5 v/v), T = 25 °C.

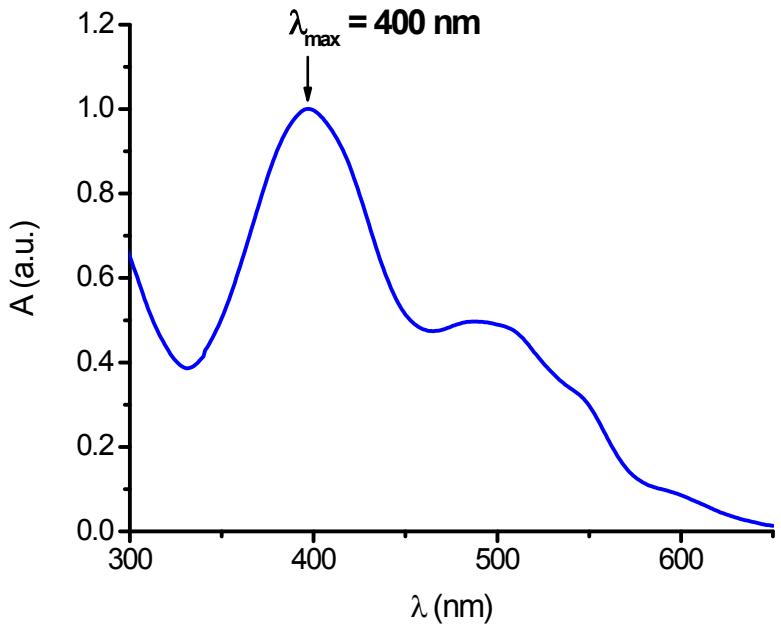

Fig. S11 Normalized absorption spectrum of compound **DXNO-BL** in H_2O:DMSO (95:5 v/v),T = 25 °C.